Research Article | Vol. 29, No. 10 / 10 May 2021 / Optics Express 14260
Optics EXPRESS

All-optical manipulation of photonic membranes

MEISAM ASKARI,[1] BLAIR C. KIRKPATRICK,[1] TOMAS ČIŽMÁR,[2,3] AND ANDREA DI FALCO[1,*]

[1]SUPA, University of St. Andrews, School of Physics and Astronomy, St. Andrews, KY16 9SS, UK
[2]Leibniz Institute of Photonic Technology, Albert-Einstein-Straße 9, Jena, 07745, Germany
[3]Institute of Scientific Instruments of CAS, Královopolská 147, 612 64, Brno, Czech Republic
*adf10@st-andrews.ac.uk

Abstract: We demonstrate the all-optical manipulation of polymeric membranes in microfluidic environments. The membranes are decorated with handles for their use in holographic optical tweezers systems. Our results show that due to their form factor the membranes present a substantial increase in their mechanical stability, respect to micrometric dielectric particles. This intrinsic superior stability is expected to improve profoundly a wide range of bio-photonic applications that rely on the optical manipulation of micrometric objects.

1. Introduction

The concept of Optical Trapping (OT) was introduced by Arthur Ashkin, who demonstrated that a spherical bead suspended in a liquid can be trapped by a strongly focused Gaussian beam, due to the balance of scattering and gradient forces [1–4]. Today, OT is a versatile tool that is capable of exerting and measuring forces from fN to several nN [5], and is a mainstream technique adopted by a diverse range of applications from biological sciences [6–8] to atomic physics [9,10]. Using OT, it is possible to directly control the position of microscopic objects, without having to rely on diffusion or the flow of liquids in microfluidic channels. Instead, the trapped objects can be driven directly into the desired place and bioprocesses triggered on demand. Examples of biological applications of OT include the manipulation of single DNA molecules and experimental assays that have enabled insight into the behavior of cells, organelles, and molecules [11–13]. In these examples, molecules or other nano-objects are grafted onto trapped spherical particles which act as handles [14,15]. Since the biological specimens are not directly trapped inside the high-intensity regions of the trapping laser field, this approach also reduces possible photodamaging effects.

To extract meaningful information on the biophysical processes of the studied objects, it is often required to monitor the position of the particle with extreme accuracy. For example, to visualize the stepping of a single enzyme moving along the DNA [16], OT is required to resolve the position of the particle within ~1 Å.

In its simplest description, an optically trapped particle behaves like an overdamped mechanical oscillator, displaced out of its equilibrium by the Brownian Motion (BM) to which it is subjected [17,18]. Since BM has zero average, to reduce its effect it is sufficient to track the position of the particle over long times (up to several tens of seconds), sacrificing the temporal resolution. However, for longer and longer acquisition times, external sources of noise such as the drift of the system and mechanical vibrations induced by air current become more relevant. Researchers go to extreme lengths to reduce the effect of these instabilities, from compensating the stage fluctuations to hermetically sealing the whole setup in inert gas, to isolating the whole laboratory from all kinds of vibrations [19].

The stability of the particle is mostly dictated by the properties of the trapping beam (wavelength, power and numerical aperture of the objective), the refractive index contrast between the beads and the surrounding medium and the size of the beads. The uncertainty introduced by the

#420364 https://doi.org/10.1364/OE.420364
Journal © 2021 Received 21 Jan 2021; revised 1 Apr 2021; accepted 17 Apr 2021; published 26 Apr 2021

Optics EXPRESS

BM in the position of the particle is inversely dependent on the trap stiffness, which in turn is proportional to the power of the optical trapping laser. Due to its spatial profile, a focused Gaussian beam produces a stronger trap in the plane transverse to its direction of propagation. Thus, the trapped particle position fluctuates more in the laser propagation direction, and the trap stiffness in this dimension is often the limiting factor for accurate particle tracking experiments.

Intuitively, increasing the mass of the bead is a straightforward means to reduce its instability. However, for a fixed trapping power, wavelength and beam diameter, the trapping stiffness decreases for larger and larger beads, which thus are of little practical use as handles. Rather than increasing the particle's size, here we propose to change its shape, turning into a membrane. This shape naturally induces a strong inertia to movements perpendicular to its larger face, thus offering an intrinsic superior stability in this direction, respect to the spherical shape. To preserve the ability to manipulate the membrane, we decorate its corners with *lumped* handles, which can be trapped efficiently (see the sketch in Fig. 1). This approach is traditionally used to manipulate optically complex shapes with added functionalities [20,21], from surface profilers [22], to steerable waveguides [23], microscopic pipettes [24], and inorganic nano-sheets [25].

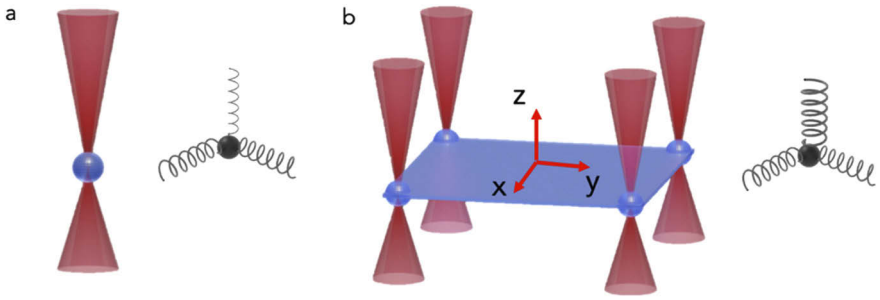

Fig. 1. Sketch of optical trapping. a) For spherical beads, the trap stiffness along the direction of propagation of the trapping beam is weaker than in the transversal direction. b) PMs presents intrinsic increased stability in the longitudinal direction in comparison to spherical beads.

The use of membranes in optical tweezing introduces additional, unique appealing features. Because of their planar configuration, we can use the versatility of modern lithographic techniques to create Photonic Membranes (PM) with advanced capabilities. For example, it is possible to define metal features on the PM, e.g. to graft with selective chemistry molecules of interest in regions removed from the optically trapped handles, with obvious benefit in terms of reduced phototoxicity. Additionally, PMs can be built through a multi-step fabrication process, following a consolidated approach to make flexible metasurfaces on polymeric substrate [26]. This approach can be extended easily to pattern the surface of the membranes with polymeric, dielectric or metal features at the nanometers scales, to define metasurfaces with bespoke photonic functions that, combined with optical manipulation capabilities, could open new research avenues in biophotonics, e.g. for sensing [27], imaging [28] and engineering of the transfer of momentum [29].

Here we demonstrate that by decorating the PM facet with handles placed at its edges, the PM can be manipulated programmatically, by means of established holographic optical trapping (HOT) techniques. Using high speed video acquisition technique and Principal Component Analysis (PCA) [30] we studied the stability of the PMs and confirmed that they are intrinsically more stable than traditional spherical handles.

In the following, we first present the fabrication procedure of the PMs followed by the experimental results. We then present the detailed analysis of their mechanical stability and discuss their suitability for bio-oriented experiments.

Optics EXPRESS

2. Methods and materials

2.1. Fabrication

The PMs used in this experiment were fabricated in two stages. In the first stage, membranes and alignment markers were fabricated and in the subsequent phase, handles were added on top of the patterned structure. A silicon substrate was cleaned in acetone and iso-propanol using an ultrasonic bath, and a sacrificial layer (Omnicoat, Microchem) was spin-coated at 1000 RPM for 60 seconds and baked for 2 minutes at 230 °C. A 90 nm thick photo-resist layer (SU-8, Microchem) was then spin-coated at 5000 RPM for 60 seconds and soft-baked at 65 °C for 1 minute, followed by further for 4 minutes at 100 °C. The sample was patterned using a Raith eLINE Plus Electron Beam Lithography (EBL) system, with exposure dose of 2 $\mu C/cm^2$. The sample was baked after exposure at 100 °C for 2 minutes and developed in Ethyl Lactate solvent for 45 seconds. After development, the alignment markers were covered using dicing tape and a 1.5 µm thick SU-8 layer was deposited on the substrate and baked for 10 min, ramping the temperature from 65° C to 95 °C. The handles were then defined via EBL with a dose of 5 $\mu C/cm^2$, followed by the same post-exposure and development procedure used for the membranes. MF-319 (MicroChem) was finally used to remove the sacrificial layer and release the PM structures into a vial. The MF-319 was gradually diluted, adding deionized water to the solution and extracting the liquid from the top layer of the vial, until fully replaced. After the lift-off, the solution containing the membranes was placed in a standard microfluidic chamber for the experiments. A sketch of the fabrication procedure is shown in Fig. S1 of the Supplement 1.

2.2. Experimental setup

For the trapping experiments, we developed a custom setup based on a standard HOT configuration, consisting of a LuxX compact CW diode laser, (Omicron) operating at 830 nm, with a maximum output power of 230 mW. A 10x telescope was used to expand the laser beam and fill the active area of the spatial light modulator (SLM, Boulder Nonlinear Systems 512×512). A 4f system was built to relay the holographic pattern placed on the SLM to the back aperture of the objective lens. An inverted microscope layout with a water-immersion, high-numerical-aperture objective lens (Olympus UPLSAPO 60XW) was used to trap the beads and membranes tens of microns away from the coverslip, where additional friction effects can be neglected. The setup was controlled with a LabView virtual instrument, providing a graphical user interface for the end-user. The analysis was done using a high-speed video acquisition technique, using a Basler piA640-210gm CMOS camera. By restricting the sensor area to an array of 50 by 50 pixels, the video acquisition rate was increased to 1000 frames per second.

3. Results

The yield of the process is very high and a typical sample with an area of $1cm^2$ contains in excess of 100 K PMs. Figure 2(a) shows a scanning electron microscope image of a uniform PM with square handles and Fig. 2(b) shows PMs of different scales and with different motifs built into them, after EBL exposure and development. Using the HOT, a trap per corner was generated, and the PMs were manipulated by addressing the four traps individually. We demonstrate this control by moving the PM through the microfluidic environment in a fully automated sequence of steps, as shown in the Visualization 1. Keyframes from this sequence are shown in Fig. 2(c)-(f). To aid the eye in distinguishing PM orientation, a one-dimensional grating was added to its surface.

To characterize the optomechanical dynamics of the PM, we used a plain, untextured membrane with a side of 15 µm and square handles with sides of 2 µm. To track its position in time, we fixed to its surface a bead of 1 µm diameter (as shown in Fig. S2). This approach guarantees a straightforward quantitative assessment of the motion of the membrane, which relies on the well predictable scattering of the spherical bead. In the following, when referring to the dynamics

Optics EXPRESS

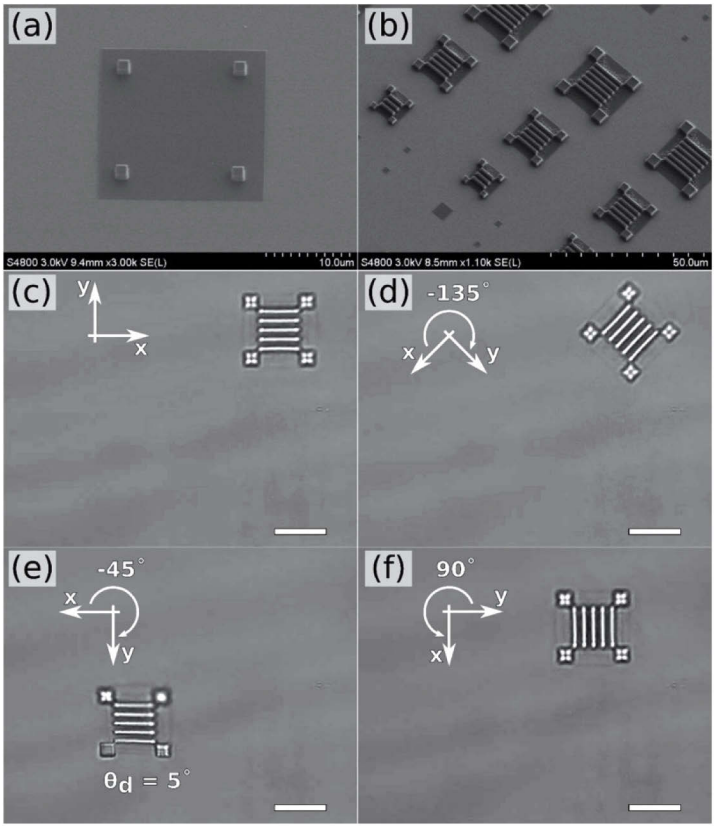

Fig. 2. (a) SEM picture of a uniform membrane, (b) SEM picture of an array of PMs with a 1D grating pattern. (c)-(d) Keyframes of the actuated PM. (c) The PM is in the start position, trapped via one optical trap per handle (traps not visible). (d) The PM is rotated clockwise about the optical axis of the trapping beam through an angle of 135°. (e) The PM is then translated through the sample and tilted out of the plane by approximately 5°. Held in this orientation, it is then rotated about the optical axis through a further 45°. (f) Finally, the PM is brought back parallel to the XY plane and then rotated through 90° while being translated back towards its starting position. The scale bar is 10 µm.

of the membrane we will implicitly assume that we are indeed observing and describing the dynamics of the bead attached to it. The positions of an isolated bead of 1 µm diameter and of that of the PM were tracked in three dimensions, using video acquisition with the camera, and a custom-built algorithm, based on the shift property of Fourier transform and PCA [30]. A typical reconstructed trace of the position in space vs time is shown in Fig. 3(a), for a trapping laser power of 4 mW, measured directly after the microscope objective. In the case of the membrane, the power was distributed equally across the 4 handles, which were individually trapped with 1 mW each. It is particularly instructive to create a scatter plot of these trajectories, as shown in Fig. 3(b) for both the bead and the membrane. To avoid crowding the figure, we selected a 2s period of the traces, greyed out in Fig. 3(a).

Optics EXPRESS

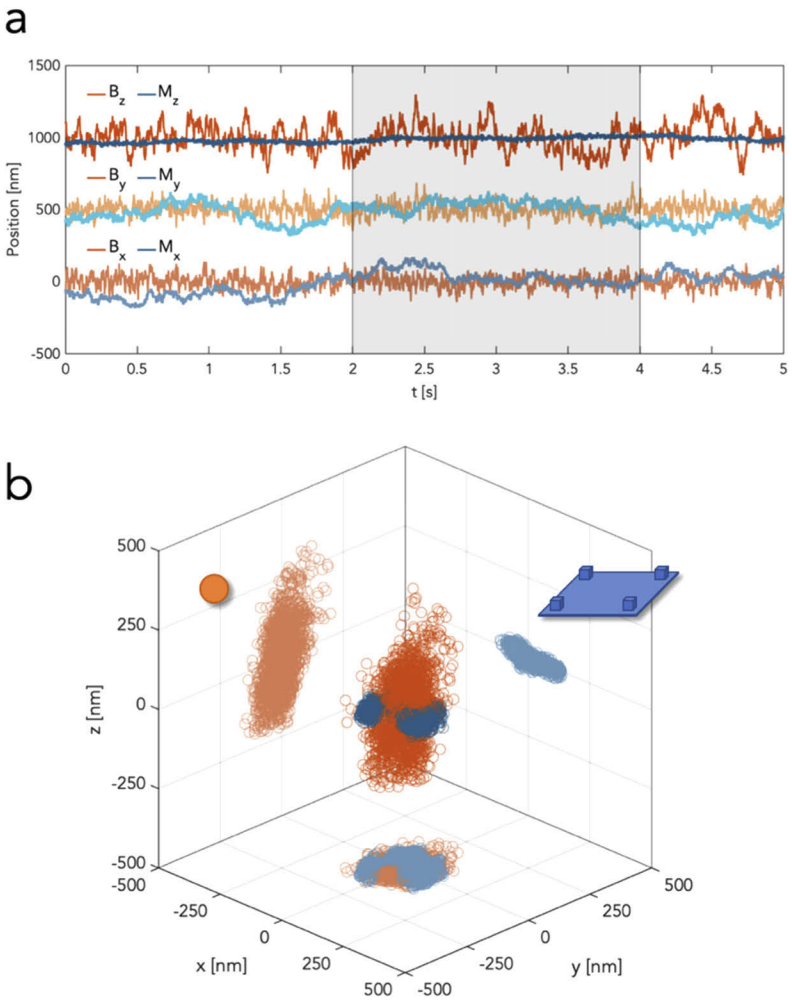

Fig. 3. (a) Trajectory in X, Y and Z directions vs time of the bead and of the PM. (b) Scatter plot of the trajectories of the particle (in orange) and of the membrane (in blue).

4. Discussions

In the following analysis, we will assume that the motion of the membrane is well described by the standard formulation of the Langevin equation [31]. However, since the dynamics are dictated by the form factor of the PM, the hydrodynamic drag coefficient of a sphere cannot be used to describe the motion of the fiducial bead attached to the PM. Nonetheless, the typical figures of merit that describe the motion of an optically trapped object can be extracted from the trajectories shown in Fig. 3(a). To this extent, for simplicity's sake, we assume that the motion of the membrane is substantially unaffected by the bead attached to it. Additionally, the membrane is assumed not to be deformable and only subject to rigid translations. A qualitative investigation of Fig. 3(a) suggests readily that the PM is more subjected to low frequency and relatively large departures from its equilibrium position respect to an isolated bead. On the other hand, high-frequency oscillations appear to be substantially suppressed. This can be better appreciated in the scatter plots of the positions of both an isolated bead and a PM shown in Fig. 3(b), which corresponds to a 7.5-fold reduction of the standard deviation of the dynamics in the direction

Optics EXPRESS

perpendicular to the direction of propagation of the trapping beam. It should be noted that for higher and higher trapping power this *advantage* reduces (doubling the power of the trapping beam reduces this factor to ~5x). However, in most biological assays it is particularly important to keep the optical power at its minimum, to avoid depositing large optical energies in close proximity to the analyte of interest. For the same reason, it is not desirable to use large beads as handles, which would yield reduced instability at the cost of a much weaker trap stiffness, hence much higher operational powers. Fig. S3 shows the scatter plot of the coordinates of the PM compared to that of trapped beads of different size and mass. Fig. S4 shows similar plots for PMs of different side length. Fig. S5 shows the trajectories along Z vs time for several PMs, confirming the consistency of the results. These initial considerations encapsulate the most striking difference between these two optically trapped objects and motivates the rationale for considering the PM as a valid platform in optical trapping for biophotonics applications.

A more quantitative analysis can be completed extracting the power spectral density (PSD) from the trajectories of Fig. 4, which are described by the analytical formula $P(f) = \frac{k_B T}{2\pi^2 \gamma} \frac{1}{(f^2+f_c^2)}$. Here, f is the frequency, γ is the friction coefficient at the temperature T, k_B is the Boltzmann constant, $f_c = k(2\pi\gamma)^{-1}$ is the corner frequency, which is given by the ratio between the spring constant k and γ. From a physical point of view, for frequencies below f_c, the motion of the object is determined by the trap potential. For frequencies higher than f_c the dynamics is diffusive and driven by the BM. Remembering that the Einstein diffusion coefficient is $D = k_B T \gamma^{-1}$, when plotted in log-log scale the PSD shows a plateau for low frequencies at a value $D(2\pi^2 f_c^2)^{-1}$ and a high-frequency behavior dictated by the term $D(2\pi^2 f^2)^{-1}$.

For the case of the isolated bead, the tracking along the longitudinal direction was calibrated assuming that the diffusion constant of the bead is the same in all directions. A fit of the PSD shown as dashed lines in Fig. 4 gives a diffusion constant D=0.48μm^2/Hz and a trap stiffness of $k_{x,y}$=2 fN/nm and k_z=0.41 fN/nm, in the transverse and longitudinal direction respectively. These values are in line with what expected by a HOT system, given the low power and the fact that we didn't adopt any elaborate strategy to increase the stability of the system. In Fig. S6 we show that k_x increases linearly with the trapping power, as expected for well-behaved setups. The PSD of the membrane trajectories does not show obvious trapped dynamics, despite the evidence that PMs can be manipulated effectively in the medium (as witnessed by the video in the SI). This is mostly due to reaching the noise floor of our system. Despite this shortcoming, the analysis of the PSD can be used to extract the diffusion coefficients for the PM, relying on the calibration of the tracking procedure completed for the isolated bead case. Due to the form factor of the PM, these vary from a value of D_{xy}=0.01 μm^2/Hz to D_z=1e^{-4} μm^2/Hz, for the transverse and longitudinal directions, respectively. These values are obtained from the fit of the $1/f^2$ slopes of the PSD. Most remarkably, already at a frequency of ~10 Hz, the dynamics of the membrane is so stable that goes below the detection limit of the system, as witnessed by the flattening of the PSD in the z-direction of the PM, shown in the third panel of Fig. 4(a).

To evaluate the usability of the PM as a stable macro-handle for bio-photonics experiments, it is useful to use the trajectories in Fig. 3(a) to calculate the Mean Square Displacement (MSD) as a function of the time interval τ, which gives a measure of the displacement within a given lag time of the trapped object from its equilibrium position. Due to the action of the trapping potential, a trapped object will remain in proximity of its original position, with an average distance dictated by the trap stiffness. Figure 4(b) shows that after an initial period proportional to $2D\tau$, in which the trapped objects diffuse due to the BM, they reach a plateau, with value inversely proportional to the trap stiffness. In Fig. 4(b), we marked these values for the isolated beads, using the same parameters extracted by the fit of Fig. 4(a), without any additional adjustment, showing an excellent agreement between the different methods of analysis. From the MSD of the membrane, it is clear that the PM has a somewhat less straightforward behavior. The dynamics along the transverse direction only plateaus around 1 s, at an intermediate trap stiffness between $k_{x,y}$ and

Optics EXPRESS

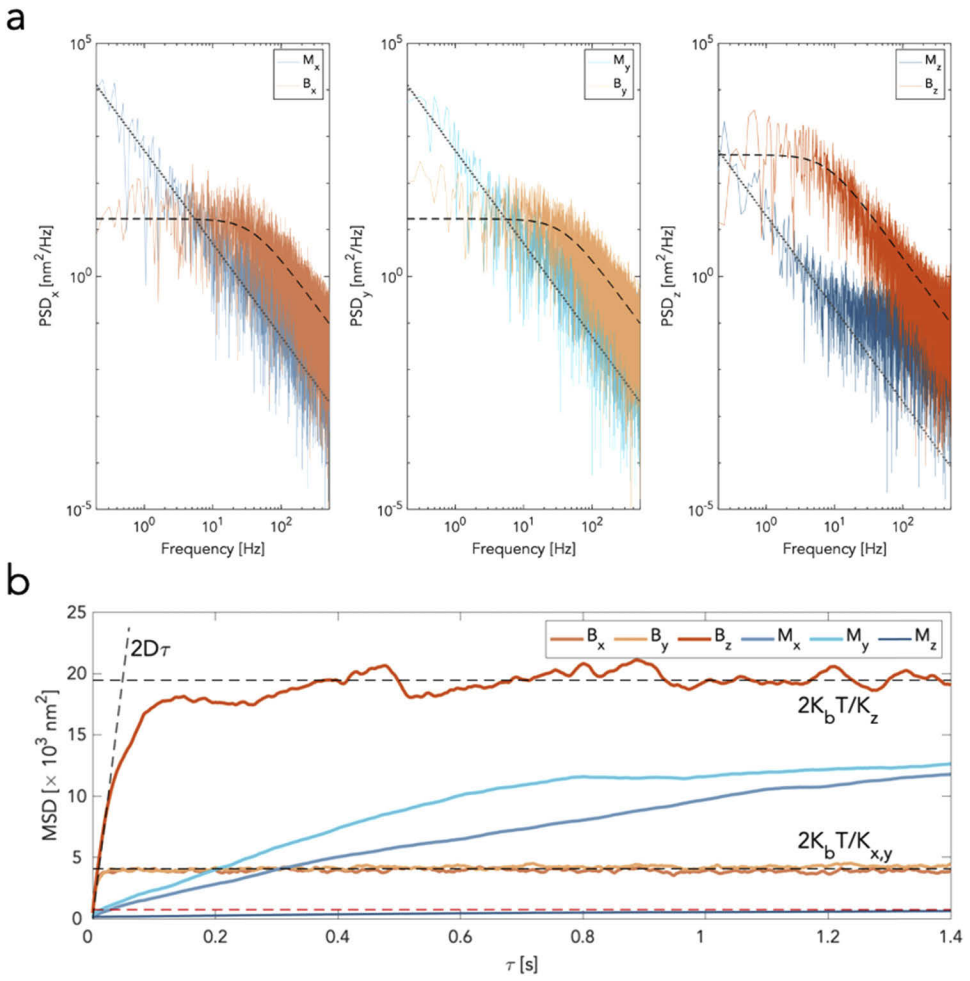

Fig. 4. Panel (a) shows the power spectral density signal of the isolated bead in orange and of the trapped PM in blue along different directions. The dashed black line is the Lorentzian fit of the PSD signal of the trapped bead. The dotted black lines are the $1/f^2$ fit of the PSD of the membrane. Panel (b) shows the MSD signal for the trapped membrane and particle. After the initial diffusion period, the MSD of the trapped particle in Z plateaus at a much higher value compared to that of the membrane, marked with a red dashed line.

k_z of the bead. In comparison, the PM appears to be more stable along the z direction, with an MSD roughly 40 times lower than that of the isolated bead. The comprehensive analysis of the trajectories, PSD and MSD of the motion of the PM compared to that of an isolated bead provides a clear insight into the different type of dynamics that governs them. Whereas an isolated bead moves very quickly in all directions and needs to be trapped with highly focused and relatively high-power beams to be stabilized, a PM tends to move very slowly and is very stable even at extremely low pumping power. However, this also means that while for a bead it is possible to average out the noise simply by acquiring its trajectory over longer and longer periods, a PM is more exposed to the effects of slow and long terms noise factors. Therefore, PM appears to be particularly promising for experiments that require very short acquisition times at low trapping power [32,33].

Optics EXPRESS

While a detailed study of how the geometry of the PMs influences its stability goes beyond the scope of this work, Fig. S4 indicates that smaller membranes tend to be more easily stabilized by the optical traps and hence manipulated more effectively. Conversely, larger membranes tend to exhibit a larger intrinsic stability, since they are heavier and wider, at the cost of reduced trap strength. These considerations can inform the choice for the most suitably sized PM, in relation to the type of experiment, the constraint on power budget and required stability.

5. Conclusion

In conclusion, PM structures fabricated using EBL were suspended in water and manipulated using HOT. We demonstrated that by designing PMs with appropriate handles, it is possible to achieve 6 degrees of freedom in the manipulation of the PM in the microfluidic chamber. Using PSD and MSD methods, we analyzed the trapping stability of the spherical particle and PM structure and we reported that the stability of the PMs in the laser propagation direction is far superior to that of the trapped particle. Using PCA we extracted the trajectories of the particles and of the PMs in time and space, and we established that in the laser propagation direction, the PM stability is almost 8 times better than that of a spherical particle with diameter of 1 μm. We anticipate that all optically manipulated PMs with enhanced intrinsic stability and advanced photonic response will have a strong impact in future biophotonic experiments and applications.

Funding. European Regional Development Fund (CZ.02.1.01/0.0/15_003/0000476); European Research Council (724530, 819346).

Acknowledgements. We acknowledge support with the experimental setup from Tomasz Plaskocinski and Yoshiko Arita. BC and MA fabricated the sample and collected the experimental data. MA, TC and ADF completed the data analysis. TC and ADF supervised the project. ADF wrote the manuscript with contribution from all authors.

Disclosures. The authors declare that they have no conflict of interest.

Data availability. The data underpinning this work can be accessed at https://doi.org/10.17630/026e2f5a-0c28-4423-9661-d0f954a58f98

Supplemental document. See Supplement 1 for supporting content.

References

1. A. Ashkin, "Trapping of Atoms by Resonance Radiation Pressure," Phys. Rev. Lett. **40**(12), 729–732 (1978).
2. A. Ashkin, J. M. Dziedzic, and T. Yamane, "Optical trapping and manipulation of single cells using infrared laser beams," Nature **330**(6150), 769–771 (1987).
3. A. Ashkin, "Applications of laser radiation pressure," Science **210**(4474), 1081–1088 (1980).
4. A. Ashkin, J. M. Dziedzic, J. E. Bjorkholm, and S. Chu, "Observation of a single-beam gradient force optical trap for dielectric particles," Opt. Lett. **11**(5), 288–290 (1986).
5. F. Czerwinski, A. C. Richardson, and L. B. Oddershede, "Quantifying noise in optical tweezers by allan variance," Opt. Express **17**(15), 13255–13269 (2009).
6. S. M. Block, D. F. Blair, and H. C. Berg, "Compliance of bacterial flagella measured with optical tweezers," Nature **338**(6215), 514–518 (1989).
7. S. M. Block, "Making light work with optical tweezers," Nature **360**(6403), 493–495 (1992).
8. K. Svoboda, C. F. Schmidt, B. J. Schnapp, and S. M. Block, "Direct observation of kinesin stepping by optical trapping interferometry," Nature **365**(6448), 721–727 (1993).
9. M. J. Lang and S. M. Block, "Resource Letter: LBOT-1: Laser-based optical tweezers," Am. J. Phys. **71**(3), 201–215 (2003).
10. J. E. Molloy and M. J. Padgett, "Lights, action: Optical tweezers," Contemp. Phys. **43**(4), 241–258 (2002).
11. V. Bormuth, A. Jannasch, M. Ander, C. M. van Kats, A. van Blaaderen, J. Howard, and E. Schäffer, "Optical trapping of coated microspheres," Opt. Express **16**(18), 13831–13844 (2008).
12. D. G. Glass, N. McAlinden, O. R. Millington, and A. J. Wright, "A minimally invasive optical trapping system to understand cellular interactions at onset of an immune response," PLoS One **12**(12), e0188581 (2017).
13. I. A. Favre-Bulle, A. B. Stilgoe, E. K. Scott, and H. Rubinsztein-Dunlop, "Optical trapping in vivo: theory, practice, and applications," Nanophotonics **8**(6), 1023–1040 (2019).
14. L. Kuyper and D. T. Chiu, "Optical Trapping: A Versatile Technique for Biomanipulation," Appl. Spectrosc. **56**(11), 300A–312A (2002).
15. S. P. Gross, "Application of optical traps in vivo," Methods Enzymol. **361**, 162–174 (2003).
16. T. T. Perkins, "Ångström-Precision Optical Traps and Applications," Annu. Rev. Biophys. **43**(1), 279–302 (2014).

Optics EXPRESS

17. K. C. Neuman and S. M. Block, "Optical trapping," Rev. Sci. Instrum. **75**(9), 2787–2809 (2004).
18. K. Svoboda and S. M. Block, "Biological Applications of Optical Forces," Annu. Rev. Biophys. Biomol. Struct. **23**(1), 247–285 (1994).
19. E. A. Abbondanzieri, W. J. Greenleaf, J. W. Shaevitz, R. Landick, and S. M. Block, "Direct observation of base-pair stepping by RNA polymerase," Nature **438**(7067), 460–465 (2005).
20. B. Phillips, S. H. Simpson, J. A. Grieve, G. M. Gibson, R. Bowman, M. J. Padgett, M. J. Miles, and D. M. Carberry, "Position clamping of optically trapped microscopic non-spherical probes," Opt. Express **19**(21), 20622–20627 (2011).
21. D. Palima and J. Glückstad, "Gearing up for optical microrobotics: micromanipulation and actuation of synthetic microstructures by optical forces," Laser Photon. Rev. **7**(4), 478–494 (2013).
22. D. B. Phillips, J. A. Grieve, S. N. Olof, S. J. Kocher, R. Bowman, M. J. Padgett, M. J. Miles, and D. M. Carberry, "Surface imaging using holographic optical tweezers," Nanotechnology **22**(28), 285503 (2011).
23. D. Palima, A. R. Bañas, G. Vizsnyiczai, L. Kelemen, P. Ormos, and J. Glückstad, "Wave-guided optical waveguides," Opt. Express **20**(3), 2004–2014 (2012).
24. M. J. Villangca, D. Palima, A. R. Bañas, and J. Glückstad, "Light-driven micro-tool equipped with a syringe function," Light: Sci. Appl. **5**(9), e16148 (2016).
25. M. Tominaga, Y. Higashi, T. Kumamoto, T. Nagashita, T. Nakato, Y. Suzuki, and J. Kawamata, "Optical trapping and orientation manipulation of 2d inorganic materials using a linearly polarized laser beam," Clays Clay Miner. **66**(2), 138–145 (2018).
26. A. Di Falco, M. Ploschner, and T. F. Krauss, "Flexible metamaterials at visible wavelengths," New J. Phys. **12**(11), 113006 (2010).
27. A. C. De Luca, P. Reader-Harris, M. Mazilu, S. Mariggió, D. Corda, and A. Di Falco, "Reproducible surface-enhanced raman quantification of biomarkers in multicomponent mixtures," ACS Nano **8**(3), 2575–2583 (2014).
28. J. Burch and A. Di Falco, "Surface Topology Specific Metasurface Holograms," ACS Photonics **5**(5), 1762–1766 (2018).
29. O. Ilic and H. A. Atwater, "Self-stabilizing photonic levitation and propulsion of nanostructured macroscopic objects," Nat. Photonics **13**(4), 289–295 (2019).
30. I. T. Leite, S. Turtaev, X. Jiang, M. Šiler, A. Cuschieri, P. S. J. Russell, and T. Čižmár, "Three-dimensional holographic optical manipulation through a high-numerical-aperture soft-glass multimode fibre," Nat. Photonics **12**(1), 33–39 (2018).
31. K. Dholakia, P. Reece, and M. Gu, "Optical micromanipulation," Chem. Soc. Rev. **37**(1), 42–55 (2008).
32. Z. Pilát, A. Jonáš, J. Ježek, and P. Zemánek, "Effects of Infrared Optical Trapping on Saccharomyces cerevisiae in a Microfluidic System," Sensors **17**(11), 2640 (2017).
33. A. Blázquez-Castro, "Optical Tweezers: Phototoxicity and Thermal Stress in Cells and Biomolecules," Micromachines **10**(8), 507 (2019).